# Thickness dependence of surface plasmon damping and dispersion in ultrathin Ag films

Yinghui Yu, Ying Jiang, Zhe Tang, Qinlin Guo, Jinfeng Jia, Qikun Xue, Kehui Wu,* and Enge Wang
*State Key Laboratory for Surface Physics, Institute of Physics, Chinese Academy of Sciences, P. O. Box 603-20, Beijing 100080, China*
(Received 16 May 2005; revised manuscript received 1 August 2005; published 3 November 2005)

The thickness dependence of the surface plasmon damping and dispersion of atomically flat and ultrathin silver films deposited on the Si(111)-(7×7) surface was investigated by a combined high-resolution electron-energy-loss spectroscopy (HREELS) and scanning tunneling microscopy (STM) system. We found stronger plasmon energy dispersion with the momentum parallel to the surface ($q_{\|}$) in thicker films, and a significant dependence of the damping edge on the film thickness. Both of them can be associated with the presence of quantum well states (QWS) in the direction perpendicular to the film surface, which influences the interband transitions between the lower and upper 5*sp* bands of silver.

DOI: 10.1103/PhysRevB.72.205405 PACS number(s): 68.55.−a, 73.20.Mf, 68.49.Uv

## I. INTRODUCTION

Collective electron excitations at metal surfaces are central to many surface properties, such as photoemission yield and second harmonic generation. Moreover, surface plasmons can be exploited in biosensing techniques such as surface plasmon resonance (SPR) and surface enhanced Raman scattering (SERS).[1] In the past decade, high resolution electron energy loss spectroscopy (HREELS) has become a major tool for studying the surface plasmons, particularly their energy dispersion properties.[2] Two classes of metal surfaces have been intensively investigated: simple metals (Al, Mg, Na, K, Cs) and transition metals (Ag, Hg, Pd). The simple metals are model systems to test the validity of the jellium model, whose prediction of negative surface plasmon energy dispersion with the wave vector $q_{\|}$ in the long wavelength limit ($q_{\|}\sim 0$) has been verified experimentally.[2] In contrast to simple metals, silver shows positive surface plasmon dispersion and also a significant dependence on the surface orientation, indicative of strong effects of the presence of 4*d* electrons.[3,4] The surface plasmon dispersion of Ag was also found to be affected by surface interband transitions owing to the existence of surface states.[5,6]

Previous HREELS measurements of the surface plasmon dispersion on Ag were mainly performed on single crystal Ag surfaces, while HREELS data on low-dimensional Ag systems, such as ultrathin films, quantum dots and quantum wires, are still lacking. However, actual applications such as biosensing based on the SPR or SERS effects employ Ag thin films or nanodots instead of single crystals. Thus, more experimental data on low-dimensional Ag systems are desired. The ultrathin Ag film is an ideal system for studying the effects of reduced dimensionality and the quantum size effects. It has been known that atomically flat and ultrathin Ag films can be grown on the Si(111)-(7×7) surface employing a novel two-step growth technique involving a deposition at low temperature (about 100 K) followed by annealing to room temperature (RT).[7–11] The growth at low temperature results in a high nucleation density, which kinetically changes the growth mode from island growth to a layer-by-layer growth above the critical thickness (around 6 ML). Moreover, it has been well-known that the confinement of electrons in thin Ag films in the perpendicular direction results in the splitting of the *sp* band into quantum-well states (QWS's).[12] It is expected that the presence of QWS's should influence the dispersion and damping of the surface plasmons in Ag thin films. However, relevant data has not yet been reported. Previous optical[13] and HREELS (Ref. 14) measurements both reported a redshift of the surface plasmon frequency of Ag films at $q_{\|}=0$ with the increase of the film thickness. However, such dependence is not due to a quantum size effect, but rather a geometric effect, since it can be explained by a decrease of the surface-to-volume ratio with the increasing film thickness on the basis of a two-component treatment of the 5*s* and 4*d* electrons of Ag.[3]

In this paper, we systematically measured the thickness-dependence of the dispersion and damping of the surface plasmons in ultrathin silver films by HREELS and scanning tunneling microscopy (STM). We found a dependence of the plasmon damping channel with the film thickness, which can be well explained by a change of the interband transition between the QWS's and the upper 5*sp* band with the film thickness, indicative of a quantum size effect. Accordingly, the plasmon energy dispersion also shows significant thickness dependence, and possible mechanisms relative to the formation of QWS's are discussed.

## II. EXPERIMENTS

The experiments were carried out in an OMICRON ultrahigh vacuum (UHV) system consisting of a preparation chamber ($\sim 1\times 10^{-10}$ mbar) and an analysis chamber ($\sim 2\times 10^{-10}$ mbar). The analysis chamber is equipped with an OMICRON variable temperature STM, HREELS (LK-5000), low energy electron diffraction (LEED) and photoelectron emission spectroscopy (PES). The Si(111) sample was cut from a phosphors-doped (*n*-type) Si wafer with a resistivity of 2 Ω cm. The sample was flashed to about 1100 °C to obtain the Si(111)-7×7 surface, as examined by the STM. A homemade crucible was used to evaporate Ag. During the Ag film growth, the substrate temperature was kept at about 120 K by liquid nitrogen cooling. The deposition rate was monitored by a quartz-crystal oscillator to be 0.08 ML/min [1 ML refers to the atomic density of the Ag(111) plane, i.e., $1.39\times 10^{15}$ cm$^{-2}$]. After growth, the sample was transferred to the analysis chamber for STM,

 

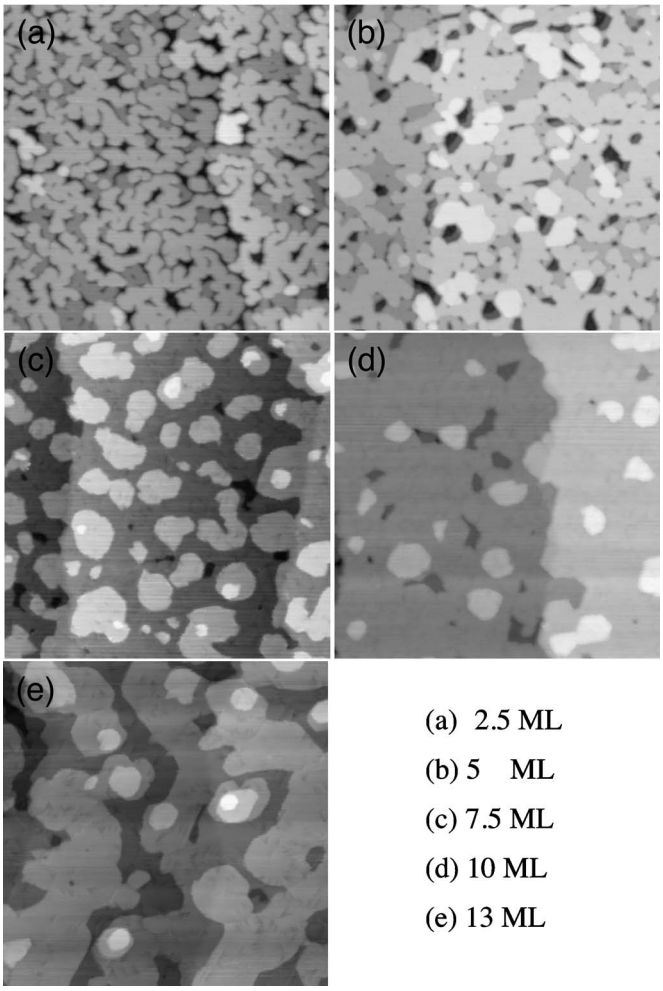


FIG. 1. STM images of Ag films with different coverages deposited on Si(111)-(7×7) at 120 K followed by annealing to RT. (a) 2.5 ML; (b) 5 ML; (c) 7.5 ML; (d) 10 ML; (e) 13 ML. The scale is 200 nm×200 nm for all images.

HREELS, and LEED measurements. Tungsten tips were used for STM imaging and all STM images were obtained at RT. The HREELS measurements were carried out at room temperature, with incident electron energy of 20 eV and an incident angle of 60° with respect to the direction normal to the surface. The dispersion of surface plasmon was obtained by rotating the analyzer around the specular direction while keeping the sample and the monochromator in fixed positions. The momentum transfer parallel to the surface $q_{\parallel}$ was calculated from the energies and angles of the incident and scattered electrons.[2]

## III. RESULTS

The typical STM images of Ag films deposited on the Si(111)-(7×7) surface at different coverages are shown in Fig. 1. As about 0.5 ML Ag is consumed in forming the wetting layer, the coverages given below are with respect to the wetting layer. As Fig. 1 reveals, below the coverage of 5 ML [(a) and (b)], silver islands with preferred-height and flat plateaus are formed, which percolate into continuous films (referred to as island growth regime). While at higher coverages [(c), (d), and (e)], the growth of Ag films becomes layer-by-layer. Our observation is in consistent with the critical thickness, 6 ML, for the change of the growth mode from island growth to layer-by-layer growth reported previously.[15] In addition, both the average size and height of the Ag islands are found to increase with the film thickness from 2.5 ML to 5 ML.

Figure 2 shows two sets of HREEL spectra obtained from two different thicknesses, 5 ML and 7.5 ML, respectively. A clear energy-loss peak can be observed with the loss energy close to that of the surface plasmon of Ag, and is therefore assigned to the plasmon excitation of the Ag film. With the increase of the parallel momentum transfer, the peak position shifts to higher energy, indicating a positive dispersion. The HREEL spectra for Ag films with different thicknesses have been obtained (not shown here), and the surface plasmon dispersion curves are plotted in Fig. 3. The parallel momentum transfer, $q_{\parallel}$, is along the $\bar{\Gamma}$-$\bar{K}$ direction of the Ag(111) surface Brillouin zone (SBZ), as measured by LEED. As seen in Fig. 3, for all different film thicknesses, the surface plasmon energy increases monotonically with increasing $q_{\parallel}$ from 0 $Å^{-1}$ to 0.3 $Å^{-1}$, with a positive dispersion at $q_{\parallel} \sim 0$. The different slopes of the dispersion curves will be discussed in detail later.

The full width at half maximum (FWHM) of the surface plasmon peaks are plotted as a function of peak energy $E_{sp}$ for different thicknesses in Fig. 4. As seen, the FWHM curves initially decreases and then increase abruptly, resulting in a well-defined critical plasmon energy ($E_{sp}^{c}$) corresponding to the minimum FWHM. More interestingly, a clear dependence of the FWHM with the Ag film thickness is observed: (1) $E_{sp}^{c}$ decreases with the increase of the film thickness; (2) the FWHM decrease with the increase of film thickness in general.

The initial decrease of FWHM has been reported for Mg (Ref. 16) and Hg (Ref. 17) films, and it is associated with effects of the lattice potential involving the increased surface barrier due to the ionic pseudopotential of the crystal and the peak broadening due to bulk interband transition including the conduction band. Similar explanation can also be applied for Ag. On the other hand, the abrupt increase of FWHM beyond the critical loss energy, $E_{sp}^{c}$, should be ascribed to the opening of a new damping channel,[2] which will be discussed in detail in the following session.

## IV. DISCUSSIONS

The FWHM of the surface plasmon peak is associated with the surface plasmon damping, as a result of its decaying into single particle excitations (Landau damping) through single 5*sp*-5*sp* band or direct 4*d*-5*sp* band transitions. The abrupt increase of the FWHM beyond $E_{sp}^{c}$, shown in Fig. 4, indicates the opening of a new efficient damping channel.[2] Figure 5(a) shows the band structure of Ag along major symmetry directions.[18] The Ag 4*d* bands are located at energies 4–8 eV below the Fermi level. Between the 4*d* bands and the Fermi level is the free-electronlike *sp* band. It crosses the Fermi level along [100] and [110], but leaves a small gap

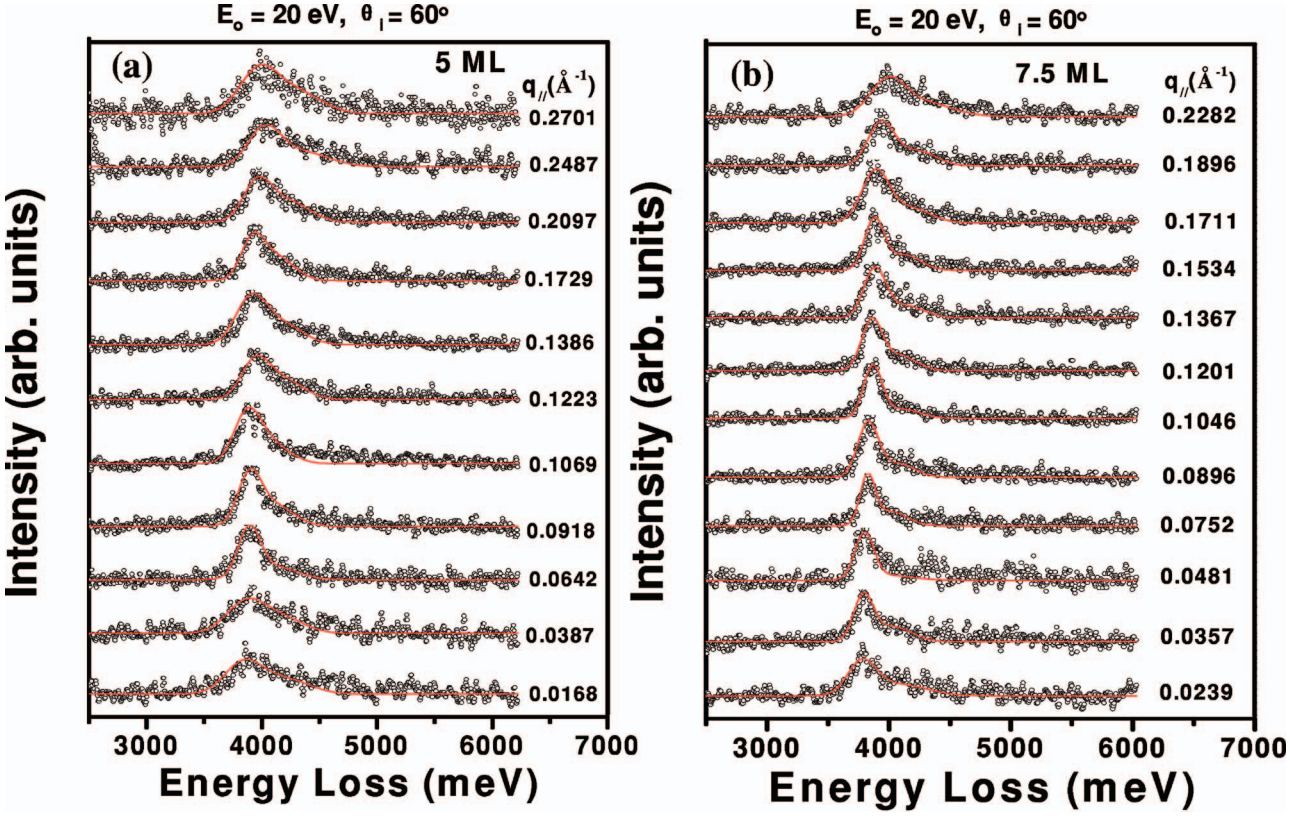


FIG. 2. (Color) Two sets of HREEL spectra obtained at different scattering angles $\theta_s$ for Ag film thickness at 5 ML and 7.5 ML, respectively. An electron primary energy $E_0=20$ eV and an incident angle $\theta_s=60°$ were used. The Gaussian fitting for each curve is also shown in the figure.

(0.3 eV) along the [111] direction, the direction perpendicular to the present Ag(111) film surface. The direct *sp*-*sp* interband transition energy at the $L$ point of the BZ is 3.86 eV,[19] which well coincides with $E_{sp}^{c}$ (3.82–4.02 eV) observed in our experiment. Thus, the observed abrupt increase of the FWHM beyond $E_{sp}^{c}$ in our experiment most likely corresponds to the opening of *sp*-*sp* interband transition channel.

To understand the thickness dependence of $E_{sp}^{c}$, we refer to the formation of QWS's in the Ag films. As is well known that the confinement of the *sp* electrons within the film thickness in the perpendicular direction results in quantization of the *sp* band into QWS's,[12] we propose that the *sp*-*sp* interband transition can also be affected by the formation of QWS's. Figure 5(b) shows the QWS's with the quantum number $n=1$ in the [111] direction (the $\Gamma$-$L$ direction of the BZ). The QWS of a thinner film lies below that of a thicker film.[20] On the other hand, because the surface plasmon has only parallel momentum ($q_{\parallel}$) and lacks in the perpendicular momentum ($q_{\perp}$), the interband transitions excited by the surface plasmon can only be constant-$k_{\perp}$ transition, i.e., a vertical transition in Fig. 5(b). It is clearly shown in Fig. 5(b) that the transition energy in a thinner film is larger than that in a thicker film, which explains the observed thickness dependence of the FWHM.

To be more quantitative, the in-plane dispersion of the QWS's should be considered. Figures 5(c) and 5(d) show a schematic drawing of the in-plane energy dispersion of the QWS with the quantum number $n=1$ and the corresponding final states in the upper *sp* band in Fig. 5(b) for two different film thickness. The in plane direction is along the $\bar{\Gamma}$-$\bar{K}$ direction of the SBZ. Because the dispersion of the upper *sp* band along the $\bar{\Gamma}$-$\bar{K}$ direction is much smoother than the lower *sp* band,[21] the onset of the 5*sp*-5*sp* interband transitions ($\omega_{T1}$ and $\omega_{T2}$) occurs at the vicinity of the Fermi level. In the case of $q_{\parallel}=0$, the transition is constant-$k_{\perp}$ transition and thus vertical in Fig. 5(c), while for a finite parallel momentum transfer ($q_{\parallel}\neq 0$), the transition is no longer vertical. In order to simplify this condition and make it more intuitive, the QWS band can be rigidly shifted by $q_{\parallel}$ along the $\bar{\Gamma}$-$\bar{K}$ direction and then artificially consider the transition as vertical,[22] as shown in Fig. 5(d). As seen, because of the small dispersion of the upper *sp* band, critical transition energy is approximately determined by the energy of the final states in the upper *sp* band at the $\bar{\Gamma}$ point, $E_f$, which in turn is determined by the dispersion of the upper *sp* band in the $\Gamma$-$L$ direction.

According to the two-band model the dispersion of the upper *sp* band along the $\Gamma$-$L$ direction can be given by Eq. (1),[18]

$$E(k_{\perp}) = E_0 - \frac{\hbar^2}{2m_f}(k_{\mathrm{BZ}} - k_{\perp})^2 - U + \left(4\frac{\hbar^2 k_{\mathrm{BZ}}^2}{2m_f}\frac{\hbar^2(k_{\mathrm{BZ}} - k_{\perp})^2}{2m_f} + U^2\right)^{1/2}, \quad (1)$$

where $U=4.2$ eV is the band gap at the $L$ point of Ag(111),

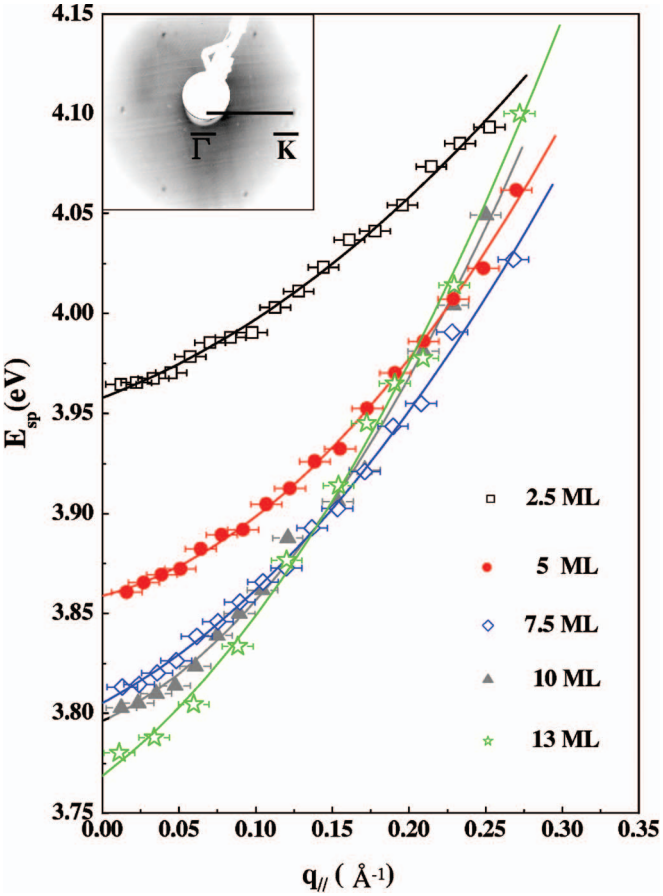


FIG. 3. (Color) The surface plasmon dispersion versus the parallel momentum $q_{\parallel}$ for different Ag coverages. The best-fitting curves for the dispersion are also displayed. The error bars indicate the finite angular acceptance of the HREELS analyzer, which is typically 1° corresponding to 0.02 $Å^{-1}$ in the momentum space. The inset is the LEED pattern where the surface Brillouin zone of Ag(111) is indicated.

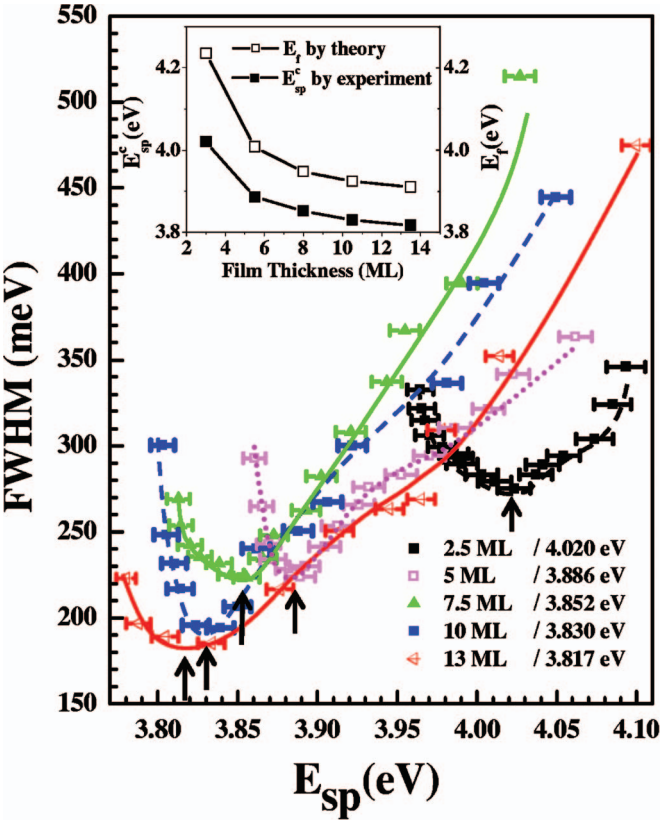


FIG. 4. (Color) The FWHM of the surface plasmons as a function of the plasmon energy $E_{sp}$ for different film thickness. The critical plasmon energy $E_{sp}^{c}$ corresponding to the minimal FWHW is indicated by a black arrow. The inset in the figure shows the comparison between the $E_{sp}^{c}$ and theoretically calculated energy of the final states (in the $\Gamma$-$L$ direction) corresponding to the quantum number $n=1$. Note that because the data of dispersion in the $\bar{\Gamma}$-$\bar{K}$ direction is not available, only the line shapes of the two curves should be compared. The overall profile of the curve nicely agrees with the experiment.

$E_0=3.86$ eV is the position of the edge of the upper *sp* band relative to $E_F$, $m_f$ is the effective mass of electrons in the upper *sp* band, $k_{BZ}=1.33$ $Å^{-1}$ is the wave vector at the BZ boundary (the $L$ point in the $\Gamma$-$L$ direction). As shown in Fig. 5(b), the final state to which the electron is excited has the same $k_{\perp}$ as the initial QWS. For quantum number $n=1$, $k_{\perp}=k_{BZ}-\pi/d$, where $d$ is the thickness of the Ag films (the phase shifts at the interfaces are neglected). The energies of the final states corresponding to the initial QWS with $n=1$ for different film thickness are calculated, as shown in the inset of Fig. 4. The profile of the final state energies agrees nicely with our experiments of the critical plasmon energy, supporting the validity of our model. The curve fitting gives an effective mass of $1.7m_e$. The slight deviations at 2.5 ML can be explained by the roughness of the film morphology. In addition, in the case of 2.5 ML, the plasmon energy is rather high (>3.94 eV, the onset of *d-sp* transition), the *d-sp* transition may play a role in the surface plasmon damping, resulting in the deviation of $E_{sp}^{c}$ from our calculation.

In what follows we consider the energy dispersion of the surface plasmon with the parallel momentum transfer $q_{\parallel}$. The surface plasmon dispersion curves in Fig. 3 can be fitted by a linear term and a quadratic term: $E_{sp}=A+Bq_{\parallel}+Cq_{\parallel}^{2}$. The best-fitting parameters are shown in Table I. According to the overall profile of these curves, the parallel momentum $q_{\parallel}$ can be qualitatively divided into three regions: the center of the SBZ ($q_{\parallel}=0$), long wavelength region (small $q_{\parallel}$), and the region of large $q_{\parallel}$.

At $q_{\parallel}=0$, there is a redshift of the surface plasmon energy with the increase of the Ag film thickness, as shown in Fig. 3. The result is inconsistent with previously reported optical and HREELS experiments on thin Ag films,[13,14] and can be well explained by Liebsch's *s-d* mutual polarization model.[3,4] As the *s-d* electrons interaction results in the reduction of the plasmon energy from the free-electron value of 6.4 eV to the actual one of 3.7 eV, the weaker *s-d* electron interaction implies the higher plasmon energy. Because the *d* electrons have smaller interaction with the free electrons in the spill out region, increasing the surface to the volume ratio will result in a decrease of the *s-d* electron interaction, and thus a blueshift of the plasmon energy. As can be seen in our STM images in Fig. 1, the growth of Ag film can be divided into two regimes. In the island growth regime (<6 ML), the

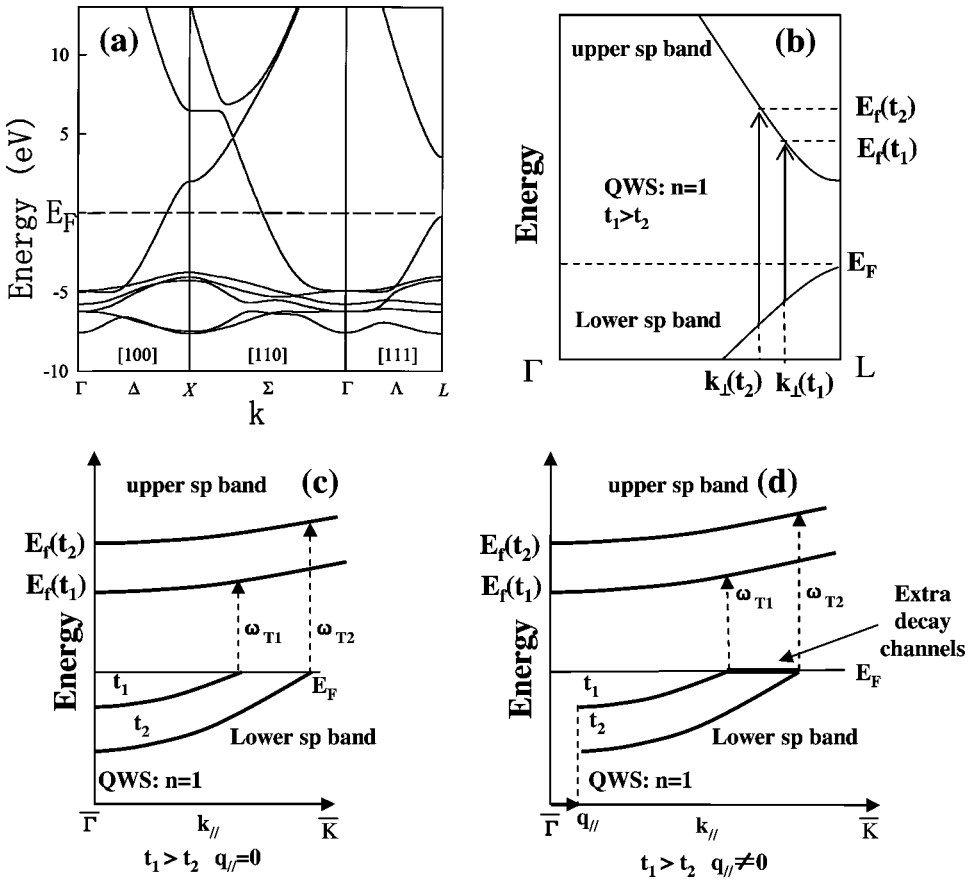


FIG. 5. (a) The band structure of Ag along major symmetry directions. (b) The zoom-in view of the *sp* bands in the Γ-*L* direction of the BZ. Two QWS's with the quantum number $n=1$, at different film thickness, $t_1 > t_2$, are marked in the lower *sp* band as $k_\perp(t_1)$ and $k_\perp(t_2)$. In the surface plasmon damping, electrons jump from these QWS's to the upper *sp* band whose final energies are represented by $E_f(t_1)$ and $E_f(t_2)$. (c) The in-plane dispersion of the QWS's and the dispersion of the corresponding final states in the upper *sp* band along the $\bar{\Gamma}$-$\bar{K}$ direction. The $\omega_{T1}$ and $\omega_{T2}$ represent the onsets of the interband transitions and $\omega_{T1} < \omega_{T2}$ can be concluded for $t_1 > t_2$. (d) is the same as (c) but with $q_\parallel \neq 0$.

surface-to-volume ratio is $1/r+1/t$, where $r$ and $t$ are the average size and height of the islands, respectively. While in the layer-by-layer growth regime (>6 ML), the surface-to-volume ratio should be $1/t$. As revealed in Figs. 1(a) and 1(b), both $r$ and $t$ of the Ag islands increase when the coverage increases from 2.5 ML to 5 ML. Thus, the surface-to-volume ratio decreases monotonically in the whole coverage regime, resulting in a redshift of the plasmon with increasing thickness.

In the long wavelength region, the linear coefficient $B$ dominates the initial slope of the dispersion curves. In Fig. 3 we observe that the initial slope of the plasmon energy dispersion curve increases with the increasing film thickness in general, although with some fluctuation within the error of curve fitting. According to the Liebsch's model, the linear term is associated with both the position of the centroid of induced charge ($d_\perp$) and the intensity of the 5*s*-4*d* mutual screening interaction.[23,24] If $d_\perp$ becomes more negative (the position of the centroid moves inward) or the 5*s*-4*d* interaction curve becomes steeper, the initial slope of the dispersion curve will increase. Since $d_\perp$ is independent on the film thickness, the slope is solely determined by the 5*s*-4*d* interaction. While the same increase in $q_\parallel$ will induce stronger reduction of the *s*-*d* interaction in the thicker film than in the thinner one due to their different surface-to-volume ratios. This leads to the larger initial positive slope in the plasmon dispersion curve in thicker films.

TABLE I. Parameters of the best-fitting function $A+Bq_\parallel+Cq_\parallel^2$ for different coverages of Ag films.

| $t$ (ML) | $A$ (eV) | $B$ (eV Å) | $C$ (eV Å$^2$) |
|---|---|---|---|
| 2.5 | 3.958 | 0.286 | 1.074 |
| 5 | 3.859 | 0.200 | 1.959 |
| 7.5 | 3.805 | 0.403 | 1.632 |
| 10 | 3.796 | 0.347 | 2.556 |
| 13 | 3.769 | 0.571 | 2.307 |

In the region of large $q_\parallel$, the induced field decays rather rapidly and the 5*s*-4*d* mutual screening interaction is almost switched off. The dispersion in this region is mainly determined by the quadratic term. As shown in Table I, the quadratic coefficient $C$ increases with the increase of the coverage in general, although with some fluctuation within the error of curve fitting. Because the interband transition suppresses the increase of surface plasmon energy, stronger interband transition indicates smaller coefficient $C$.[6] As the plasmon energies in this region are in the range from 3.8 eV to 4.1 eV, both *sp*-*sp* and *d*-*sp* transition should affect the dispersion coefficient. While the effect of *d*-*sp* transition is difficult to estimate, we suggest that the *sp*-*sp* transition is in consistent with the observed change of $C$. As seen in Fig. 5(d), for a given $q_\parallel$, the interband transition involving the QWS band below the Fermi level can influence the surface plasmon energy and give rise to a redshift of the surface plasmon energy. Moreover, for a thinner film, extra decay channels [see Fig. 5(d)] exist as compared with a thicker film, as the subband of QWS ($n=1$) for the thinner film lies below that of the thicker one. Thus the *sp*-*sp* interband tran-

sitions should be more efficient in the thinner film than in the thicker one. The interband transitions suppress the increase of the surface plasmon energy, resulting in a smaller quadratic coefficient $C$ in the thinner film than the thicker one.

Our experimental dispersion curves on ultrathin Ag films are different from the results reported by Moresco *et al.* in Ref. 14 in a similar HREELS study, although the plasmon energies at $q_{\parallel}=0$ are consistent. Particularly, they observed an absence of dispersion in small $q_{\parallel}$ range, while we observe positive dispersion in all films. There may be two possibilities for this discrepancy. (1) The morphology of the Ag films are different. Moresco *et al.* reported LEED results showing that the granular morphology of Ag islands persists even after they percolate into continuous film, resulting in the confinement of the surface plasmon inside the islands and thus the absence of dispersion in the lower $q_{\parallel}$ range. We, however, observed by STM that the Ag islands no longer maintain their complete boundaries after they percolate into continuous film. As can been seen in Fig. 1(e), only part of the boundaries exist, mainly as small-angle dislocations, which may not be sufficient to confine the surface plasmons. (2) Our measurement is performed at room temperature, while their measurements were performed at liquid nitrogen temperature. The temperature effect has to be considered in order to make more quantitative comparisons.

## V. CONCLUSION

We have systematically investigated the thickness dependence of the dispersion and damping of surface plasmon in the ultrathin Ag films. We found a dependence of the plasmon damping channel with the film thickness, which can be well explained by an influence of the *sp-sp* interband transition upon the formation of QWS's in the lower *sp* band, which shows a thickness dependence as a result of the quantum size effect. Accordingly, the plasmon energy dispersion also shows significant thickness dependence, and possible mechanisms relative to the formation of QWS's are discussed.

*Author to whom correspondence should be addressed. Electronic address: khwu@aphy.iphy.ac.cn

[1] W. L. Barnes, A. Dereuxa, and T. W. Ebbesen, Nature (London) **424**, 824 (2003).
[2] M. Rocca, Surf. Sci. Rep. **22**, 1 (1995).
[3] A. Liebsch, Phys. Rev. Lett. **71**, 145 (1993).
[4] A. Liebsch, Phys. Rev. B **48**, 11317 (1993).
[5] L. Savio, L. Vattuone, and M. Rocca, Phys. Rev. B **67**, 045406 (2003).
[6] L. Savio, L. Vattuone, and M. Rocca, Phys. Rev. B **61**, 7324 (2000).
[7] G. Meyer and K. H. Rieder, Appl. Phys. Lett. **64**, 3560 (1994).
[8] M. Hanbücken, M. Futqamoto, and J. A. Venables, Surf. Sci. **147**, 433 (1983).
[9] G. P. Chambers and B. D. Sartwell, Surf. Sci. **218**, 55 (1989).
[10] J. A. Venables, Surf. Sci. **299-300**, 798 (1994).
[11] L. Gavioli, K. R. Kimberlin, M. C. Tringides, J. F. Wendelken, and Z. Zhang, Phys. Rev. Lett. **82**, 129 (1999).
[12] I. Matsuda, T. Ohta, and H. W. Yeom, Phys. Rev. B **65**, 085327 (2002).
[13] Y. Borensztein, M. Roy, and R. Alameh, Europhys. Lett. **31**, 311 (1995).
[14] F. Moresco, M. Rocca, T. Hildebrandt, and M. Henzler, Phys. Rev. Lett. **83**, 2238 (1999).
[15] Z. Zhang, Q. Niu, and C. K. Shih, Phys. Rev. Lett. **80**, 5381 (1998).
[16] P. T. Sprunger, G. M. Watson, and E. W. Plummer, Surf. Sci. **269/270**, 551 (1992).
[17] B. O. Kim, G. Lee, E. W. Plummer, P. A. Dowben, and A. Liebsch, Phys. Rev. B **52**, 6057 (1995).
[18] T. C. Chiang, Surf. Sci. Rep. **39**, 181 (2000).
[19] P. Winsemius, F. F. Kampen, H. P. Lengkeek, and G. G. Van Went, J. Phys. F: Met. Phys. **6**, 1583 (1976).
[20] K. Pedersen, T. B. Kristensen, T. G. Pedersen, P. Morgen, Z. Li, and S. V. Hoffmann, Surf. Sci. **482–485**, 735 (2001).
[21] B. R. Cooper and Elise L. Kreiger, Phys. Rev. B **4**, 1734 (1971).
[22] P. Laitenberger and R. E. Palmer, Phys. Rev. Lett. **76**, 1952 (1995).
[23] A. Liebsch and W. L. Schaich, Phys. Rev. B **52**, 14219 (1995).
[24] A. Liebsch, *Electronic Excitations at Metal Surfaces* (Plenum, New York, 1997).